1

Introduction

1.1 ULIRGs: the last of the Mohicans

ONE of the most important extragalactic discoveries of IRAS was the detection of a class of galaxies with infrared (8–1000 μm) luminosities in excess of $10^{12}\,L_\odot$ and infrared-to-blue ratios (L_{IR}/L_B) ratios even higher than for lower luminosity infrared-bright galaxies. Except for Arp 220 and NGC 6240, none of these Ultra-Luminous Infrared Galaxies (ULIRGs) had been previously detected in optical surveys. Subsequent follow-up observations established that ULIRGs are advanced mergers, containing exceptionally large amounts of molecular gas in their nuclei (Sanders et al. 1988a,b; Kim et al. 2002; Veilleux et al. 2002). The origin of this strong infrared emission has been widely debated: the infrared luminosity may reflect intense star formation or the presence of a very active galactic nucleus (AGN). If powered entirely by star formation, ULIRGs are the most spectacular starburst galaxies in the universe, building up an entire stellar population in a few short bursts. If, on the other hand, ULIRGs are partly powered by AGN activity, the study of ULIRGs would catch the central engine in its most enshrouded phase.

Across all wavebands, enormous efforts has been made to determine the dominant power source. Such studies are greatly hampered by the presence of copious amounts of gas and dust. Outcomes are highly dependent on the AGN and starburst tracers used and often require quite a bit of faith in their applicability for strongly extincted lines of sight. This also applies to hard X-ray observations (e.g. Braito et al. 2003; Gallagher et al. 2002; Komossa et al. 2003; Lira et al. 2002; Xia et al. 2002), where, as Ptak et al. (2003) noted, “absence of evidence is not evidence of absence”. This being said, both the recent XMM and CHANDRA surveys seem to agree that starburst activity dominates over AGN activity in the nearby (z<0.045) ULIRGs that were studied (Ptak et al. 2003; Franceschini et al. 2003). For the more distant and high-luminosity ULIRGs, no such studies have yet been made.

The general evolutionary scheme emerging from all of these studies is that ULIRGs represent an important phase in the evolution of mergers. When two dust-rich spiral galaxies merge, their gravitational interaction drives gas into the galactic nuclei. After some 500 million years, this causes a strong burst of star formation at a rate of some 100 $M_\odot$/yr. The flow of gas into the nuclei may also activate the central monster. Eventually, the remaining gas has

FIGURE 1.1 — The nearby southern starburst galaxy NGC 4945 covers $20' \times 4'$ of the sky. 75% of its luminosity originates in the central $12'' \times 9''$ (Brock et al. 1988). **Left:** Despite the concentration of luminosity towards the center, the optical nucleus is inconspicuous due to strong extinction within the galaxy. Photo: ESO. **Right:** The effects of extinction are smaller in the near-infrared, permitting a glimpse of the strongly obscured nuclear starburst. Photo: Jarrett et al. (2003).

either been consumed by star formation or been shed by the powerful supernova explosions and all activity will cease. The only signs of the merger remaining may be the increased mass of the bulge and the increased mass of the central black hole (Kormendy & Sanders 1992; Genzel & Cesarsky 2000; Tremaine et al. 2002).

SCUBA and MAMBO studies have found that the number of galaxies with luminosities similar to ULIRGs was a factor 400 higher in the Early Universe compared to the Local Universe (Blain et al. 2002). As the Star Formation Rate (SFR) per comoving volume element is also found to be much higher in the Early Universe (the SFR increases from z=0 by more than a factor 10 to peak at z=1–3; Steidel et al. 1996; Lilly et al. 1996; Steidel et al. 1999), the fraction of star formation occuring in galaxies with ULIRG-like luminosities must have been far higher than in the Local Universe. As such, the ULIRGs may be the last of a dying race of merging galaxies, testament to an earlier epoch dominated by mergers, starbursts, and AGN activity. The study of nearby ULIRGs may hence allow us to probe the era when galaxies were hierachically assembled and their stars were formed.

While this general scenario is well accepted, the key question remains ”what are the relative contributions of starburst and AGN activity to the overall energetics during the various evolutionary phases of these merging galaxies ?”

1.2 Starburst in the Nearby Universe

Starburst phenomena are also known on a lessser scale in the Nearby Universe. The nearest starburst galaxy to us is M 82, at a distance of 3.3 Mpc. HST observations of the inner kpc have resolved more than a hundred compact and luminous super star clusters (de Grijs et al. 2000). The most active starburst is found in the ‘starburst core’, a region obscured by $\sim$50

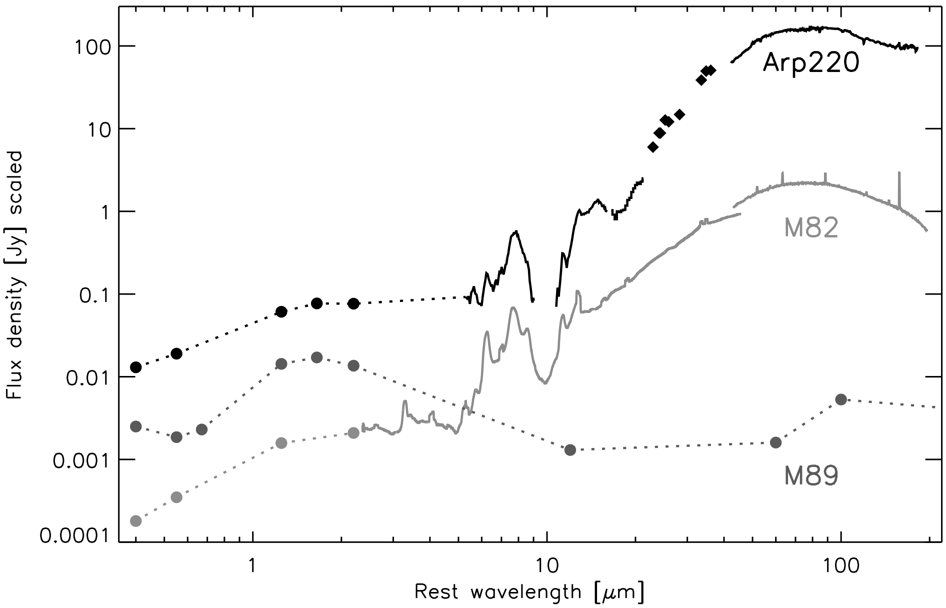

FIGURE 1.2 — Optical-infrared spectral energy distributions of M 89, M 82 and Arp 220. While the bulk of the bolometric luminosity of infrared galaxies (e.g. M 82 and Arp 220) is emitted in the mid- and far-infrared, this is not the case for most elliptical galaxies (e.g. M 89). Fluxes have been scaled and for presentation purposes, the spectrum of M 82 has been corrected for aperture effects. The ISO spectra have been taken from Fischer et al. (1997); Sturm et al. (2000); Tran et al. (2001).

magnitudes of visual extinction (Förster Schreiber et al. 2001) and responsible for most of the infrared luminosity of this galaxy. Its mid-infrared spectrum is shown in Fig. 1.9. The spectrum closely resembles the spectra of Galactic regions of massive star formation, represented in Fig. 1.9 by the spectrum of the Orion Bar (Section 1.3.1). The fierceness of the starburst is perhaps best illustrated by the presence of a nuclear bipolar outflow powered by numerous supernovae, which traces a starburst superwind out to several kpc (e.g. Lehnert et al. 1999). At the current modest star formation rate of $\sim$4 $M_{\odot}$/yr, the starburst in M 82 will run out of fuel in 60 million years, hence the name 'starburst'.

Another example of a starburst galaxy is the southern galaxy NGC 4945 (Fig. 1.1), which, like M 82, is seen nearly edge-on (i$\sim$78°). The nuclear starburst is heavily obscured at optical wavelengths, as is illustrated by the absence of an optically bright nucleus (Fig. 1.1). Unlike M 82, a powerful burried AGN lurks at the center of this galaxy, only revealing its presence in extreme hard X-rays (Iwasawa et al. 1993; Guainazzi et al. 2000).

M 82 and NGC 4945 are typical examples of 'infrared galaxies' — galaxies emitting more energy in the infrared than in the UV and optical bands combined (Soifer et al. 1984b). As infrared emission is generally dust emission, it follows that infrared galaxies are either rich in dust or efficient in heating the available dust. Infrared galaxies were discovered by the thousands by IRAS, which in 1983 surveyed 96% of the sky at mid- and far-infrared wavelengths. The survey established that the vast majority of the galaxies in the Local Universe (z<0.3) are only modest infrared emitters at $L_{\rm IR}/L_{\rm B}$ $\sim$0.4, with early-type galaxies such as M 89 rank-

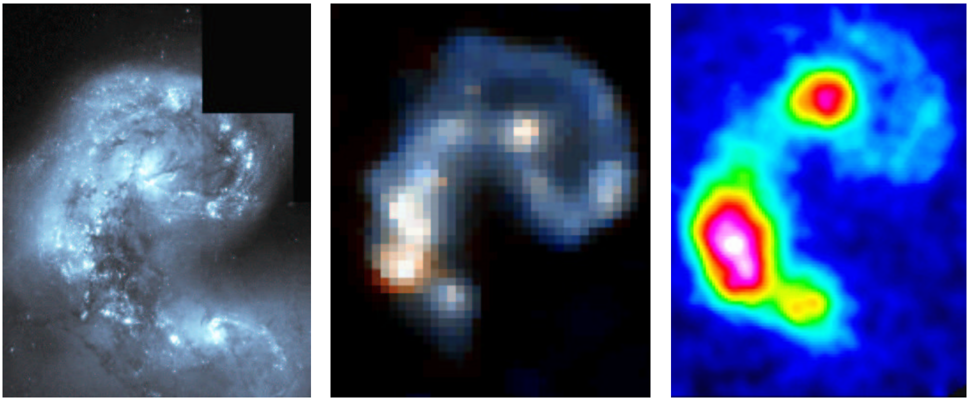

FIGURE 1.3 — "The Antennae" (NGC 4038/39) observed at three different wavelengths. **Left**: The optical image shows the distribution of stars and obscuring dust. Image: Brad Whitmore (STScI) & NASA. **Middle:** The mid-infrared image shows the interaction zone between the two nuclei to be the strongest source of warm continuum radiation. Image: ESA/ISO/ISOCAM & Laurent Vigroux. **Right:** The SCUBA image (850 μm) reveals the interaction zone to be a strong source of cold dust continuum. Image: Paul van der Werf.

ing weakest (Fig. 1.2). In contrast, classic starburst galaxies, like M 82 and NGC 253, were found to have infrared-to-blue ratios of 3 and 5 and $L_{IR}=10^{10.3}$ and $10^{10.8}$ $L_\odot$, respectively. Higher infrared-to-blue ratios, in the range of 1–50, were found for a flux-limited sample of infrared selected galaxies, a quarter of which showed clear signs of interaction (Soifer et al. 1984b). IRAS further established that most infrared galaxies with $L_{IR}<10^{11}$ $L_\odot$ are single, dust-rich spiral galaxies with no strong signs of AGN activity. Above $L_{IR}=10^{11}$ $L_\odot$, a large fraction of the galaxies were found to be strongly interacting and extremely rich in molecular gas (Sanders & Mirabel 1996).

One of the nearest (20 Mpc) and best studied examples of a Luminous Infrared Galaxy (LIRG; $L_{IR}\geq10^{11}$ $L_\odot$) is the pair of colliding galaxies NGC 4038/39, also refered to as 'The Antennae'. Wide-field optical and radio H I images reveal the galaxies to be accompanied by two 'tidal tails' extending 110 kpc in opposite directions (Hibbard et al. 2001). Structures of this kind are regarded as typical for galaxy-galaxy interactions (Toomre & Toomre 1972). In HST images (left panel of Figure 1.3), the two galaxy disks appear distorted and the two nuclei are separated by only 6.4 kpc (Whitmore & Schweizer 1995). In the overlap region between the two nuclei, strong patchy extinction coincides with a broad maximum in mid-infrared 15 μm maps (middle panel of Figure 1.3). The energy output of this region is about half of the total energy output of the system at 15 μm. As its mid-infrared spectrum shows strong resemblance to spectra of sites of massive star formation in our Galaxy, it is hence likely that the interaction has triggered a massive starburst in this region. Given the absence of equally prominent starburst emission in optical or UV maps, the example of the Antennae illustrates that UV rest frame observations of galaxies at high redshift may not probe the true star formation rate in dusty mergers. In contrast, and illustrated in the right panel of Fig. 1.3, SCUBA observations at 850 μm are more effective as a tracer of star formation (Van der Werf et al., in prep.), probing the stellar energy absorbed by dust near the peak of its spectral energy distribution.

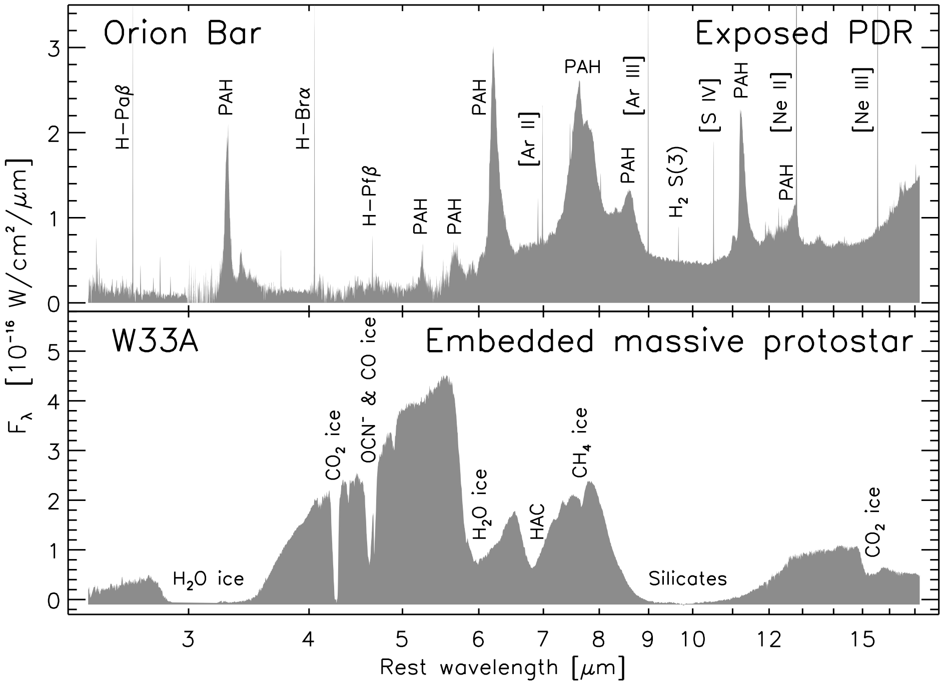

FIGURE 1.4 — Comparison of 2–17 μm spectroscopic signatures of embedded and exposed star formation. **Top panel:** Spectrum of the Orion Bar photo-dissociation region (Peeters et al. 2002a), dominated by PAH emission features at 3.3, 6.2, 7.7, 8.6, 11.2 and 12.7 μm. The emission line spectrum originates in the H II region, parts of which are included within the ISO–SWS slit. **Bottom panel:** Spectrum of the deeply embedded massive protostar W 33A (Gibb et al. 2000; Keane et al. 2001). The spectrum is dominated by deep absorption features of ices and silicates on an otherwise featureless continuum.

1.3 Characteristics of regions of massive star formation in our own Galaxy

Massive stars are formed in giant molecular clouds from small condensations which grow in mass and contract under the influence of gravity and the loss of magnetic field due to ambipolar diffusion. Eventually, after some 10^5 years, the star formation process results in the birth of a luminous embedded massive protostar. Armed with a fierce radiation field, powering a strong stellar wind, the newly born star now starts clearing a cavity around it, which turns into an H II region as a result of the irradiation with extreme-UV (EUV) stellar photons. During its expansion, the size of the H II region increases from 0.003 pc (hyper-compact) via 0.05 pc (ultra-compact) and 0.5 pc (compact) to $\sim$10 pc (extended). During this phase, the H II region will be surrounded by a Photo Dissociation Region (PDR) in which the far-UV photons from the star are absorbed by dust and neutral gas.

1.3.1 Observable characteristics

The earliest stages of star formation outlined above are extremely difficult to observe (except at submm wavelengths) as they occur in the coldest and densest parts of giant molecular

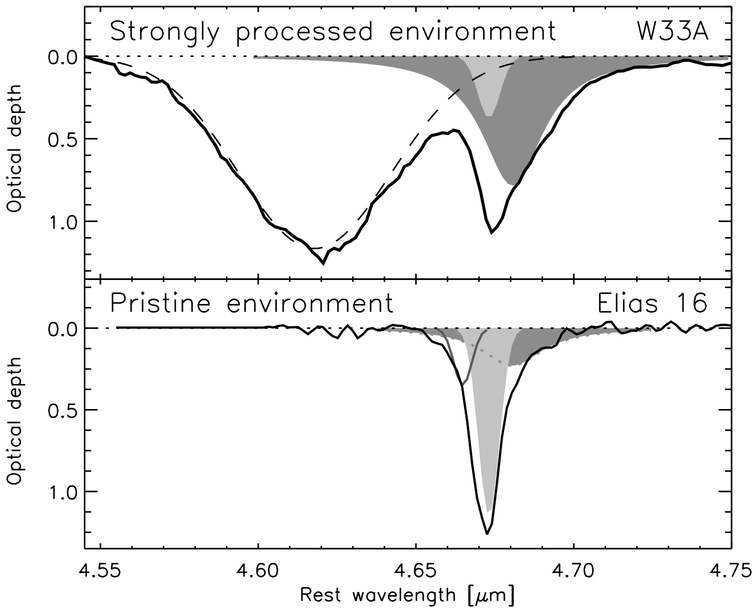

FIGURE 1.5 — Optical depth spectra (*black*)of ices in the lines of sight towards the embedded massive protostar W 33A (**top**) and the field star Elias 16, located behind the Taurus molecular cloud (**bottom**). The CO absorption feature towards Elias 16 (Chiar et al. 1995) is dominated by volatile CO ice mixtures (*light grey surface* and *dark grey line*), with a relatively small contribution of CO trapped in water ice (*dark grey surface*). In contrast, the CO absorption feature towards W 33A (Gibb et al. 2000) shows far less of the volatile CO ice mixtures and is dominated instead by CO trapped in water ice. This spectrum shows in addition a broad absorption feature due to OCN^- ice (*dashed line*).

clouds.

The first stage in the formation of massive stars which can be studied in the near- and mid-infrared is the phase in which the massive star has already reached the main sequence — while still accreting — and is heating the surrounding dust to temperatures which give rise to mid-infrared continuum emission. As the star at this stage is still buried deeply inside its parental cloud, the line of sight towards the star passes through the intervening molecular environment. This allows spectacular insight into the composition of the interstellar medium in the vicinity of newly formed stars. This is illustrated in the bottom panel of Fig. 1.4 for the massive embedded protostar W 33A. The spectrum is dominated by deep absorption features of ices, such as H_2O, CO, OCN^-, CO_2, CH_4 and CH_3OH, which are frozen onto the dust grains (Gibb et al. 2000; Keane et al. 2001). The dust grains themselves are represented by a deep absorption feature due to silicates. As the sublimation temperatures of the different ices range from 20 K to 90 K, the strengths of the respective absorption features are a good measure of the thermal processing of the interstellar medium by the forming star. Likewise, the presence or absence of certain molecules in the icy grain mantles may be taken as an indication of processing by UV photons emanating from the central source. Indicators of both types of processing are present in the rest frame M-band atmospheric window (4.55–5.05 μm): 4.62 μm OCN^- ice and 4.67 μm CO ice. Fig. 1.5 compares the optical depths

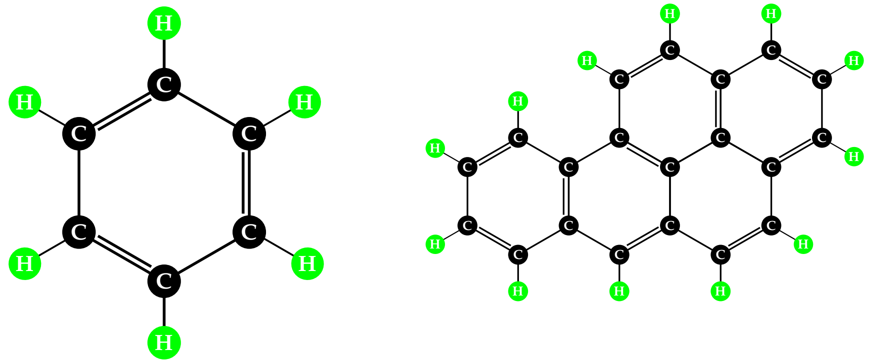

benzene **PAH molecule**

FIGURE 1.6 — Emission bands from Polycyclic Aromatic Hydrocarbons (PAHs) dominate the near- and mid-infrared spectra of star forming regions. PAHs are like other aromatic molecules, such as Benzene, toxic. Graphics: E. Peeters.

of the two features in the line of sight towards the embedded massive protostar W 33A and towards the field star Elias 16, which is located behind the Taurus molecular cloud. While OCN^- ice is absent in the quiescent Taurus molecular cloud, it is clearly present in the vicinity of the embedded protostar. Note also the shape of the CO ice absorption feature. In a quiescent line of sight (Elias 16; Chiar et al. 1995) it is narrow and dominated by volatile apolar ice mixtures containing CO, whereas towards a highly processed environment (W 33A; Gibb et al. 2000) all that is left of the feature is the red wing originating from CO ice trapped within the far less volatile water ice.

During the initial phase of the formation of the massive star, the H II region is trapped within the accreting (or outflowing) material close to the star. Eventually, however, the star will establish an H II region around it. The presence of an H II region can be detected from afar by its characteristic recombination line spectrum and radio free-free continuum emission. Especially the latter can be observed through quite a thick layer of molecular material, allowing the detection of still deeply burried young hyper and ultra-compact H II regions (Martín-Hernández et al. 2003). H II regions are surrounded by a so-called Photo-Dissociation Region (PDR; Tielens & Hollenbach 1985), in which — by definition — EUV photons from the star do not penetrate. Here we also find in addition to all kind of neutral species, dust and robust molecular species such as H_2 and CO (Tielens & Hollenbach 1985). Far-UV (FUV) photons from the star can travel freely into a PDR (subject only to absorption by dust particles which survive in the outer parts of the H II region). Here they interact with the atoms and molecules, resulting in a lively and complex chemistry. More important, however, in the context of this thesis is the possibility that FUV photons are absorbed by complex molecules known as Polycyclic Aromatic Hydrocarbons (PAHs; Fig. 1.6). These molecules, which are formed mainly in the outflows of aging low mass stars and eventually get mixed in with the general ISM, transform their UV excitation energy into vibrational energy of the molecular bonds within the aromatic structure. This results in the cooling down of the molecule, as each vibration mode produces a number of near- or mid-infrared photons in distinct bands. The main emission bands of PAHs at wavelengths of 3.3, 6.2, 7.7, 8.6, 11.2 and 12.7 μm usually dominate

FIGURE 1.7 — Detail of the Orion nebula between the four Trapezium stars (*upper left quadrant*) and the Orion Bar (*running diagonally*). **Left**: The optical image is dominated by intricate dust structures at the interface between the H II region, ionized by Trapezium star θ^1C Orionis, and the vast molecular cloud behind it. The Orion Bar is part of this interface and is seen edge-on. Its side facing θ^1C Orionis is ionized, while its far side is molecular. The transition zone, the PDR, is a major source of PAH emission (Hollenbach & Tielens 1999). Photo: NASA, C.R. O'Dell & S.K. Wong (Rice University); **Right**: The near-infrared image, taken with the ISAAC camera on the ESO–VLT, reveals the presence of an entire stellar cluster hidden within the molecular cloud. Photo: M. McCaughrean & ESO.

the near- and mid-infrared emission of PDRs. Depending on the abundance and temperature of the dust within the H II region and PDR, the PAH emission bands may also dominate the emission of the H II region and PDR combined.

A beautiful example of an H II region and associated PDR is the bright nebula centered on the Orion Trapezium stars, also known as the Orion nebula. The nebula is ionized by the young O6 star θ^1C Orionis, which, together with the other three Trapeziun stars, cleared the optically visible cavity. The four stars are the first of an entire cluster, which for the largest part is still hidden behind the cavity (Fig. 1.7). The bright ridge running diagonally accross the lefthand image of Fig. 1.7 is called the Orion Bar. This structure is part of the interface between the H II region around θ^1C Orionis and the molecular cloud and is seen edge-on. The side facing θ^1C Orionis is ionized, while its far side is molecular. Near-infrared L-band imaging reveal the interface, the PDR, to be a major source of PAH emission (Hollenbach & Tielens 1999). This is corroborated by the ISO–SWS spectrum (top panel of Fig. 1.4), which shows strong PAH emission features at 3.3, 6.2, 7.7, 8.6, 11.2 and 12.7 μm. A spectrum like this is fairly typical for exposed PDRs and, as such, distinctly different from spectra of embedded protostars, as exemplified by the spectrum of the line of sight towards the massive protostar W 33A (bottom panel of Fig. 1.4).

As discussed above, the FUV and EUV photons emitted by young hot stars are absorbed by the H II regions and PDRs around them. Observationally, these regions are thus characterized by hydrogen recombination lines, atomic fine structure lines, molecular lines, PAH emission bands and mid- and far-infrared dust continuum radiation. The latter constitutes the bulk of the re-emitted stellar luminosity, as is strikingly illustrated in Figure 1.8 by the spectrum of a typical compact H II region.

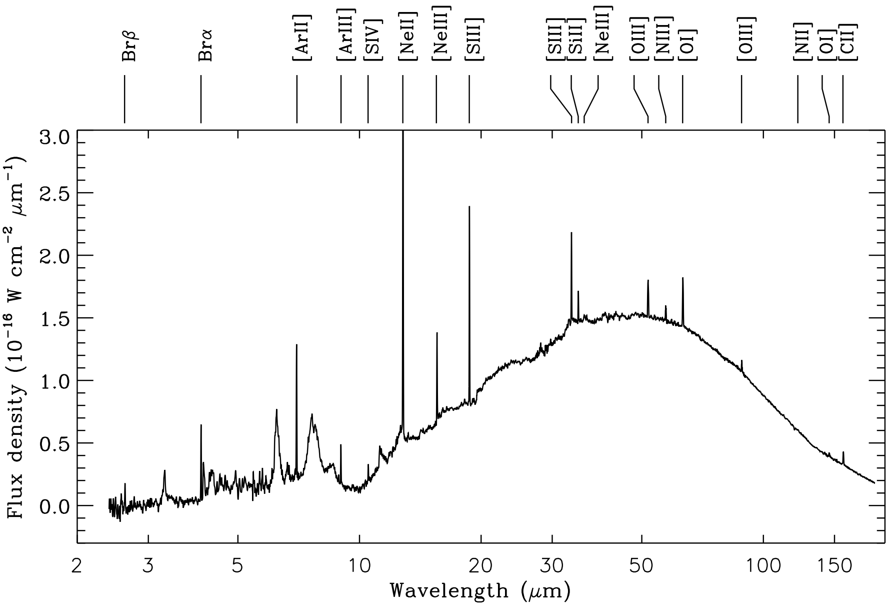

FIGURE 1.8 — The spectral energy distribution of a typical compact H II region (Peeters et al. 2002b). Most of the FUV and EUV energy of the central star is re-emitted, not in the form of hydrogen recombionation lines, fine structure lines or PAH emission bands, but in the form of mid- and far-infrared dust emission. Note the logarithmic scale on the wavelength axis, which compresses the far-infrared spectral range with respect to the near- and mid-infrared spectral ranges. Graphics: L. Martín-Hernández.

1.4 AGNs

AGNs can also be an important contributor to the energy budget of ULIRGs. The engine is hypothesized to be a super-massive black hole with a mass in the range of 10^6–10^8 $M_\odot$. It is surrounding by a fiercely X-ray emitting fast-rotating accretion disk, which in turn is surrounded by the so-called Broad-Line Region (BLR). Unification schemes interrelating the various types of active galaxies (Antonucci 1993) demand an an-isotropic dust screen to hide the central engine for type-2 AGNs. Although the dimensions of this dusty torus are not well-known, its inner radius cannot be any smaller than a few parsecs, as otherwise the dust would be destroyed by the intense X-ray emission from the accretion disk. Likewise, the outer radius of the torus cannot be much larger than a few hundred parsecs, as it would otherwise have been seen in optical images. Another important component are the gas clouds which constitute the so-called Narrow-Line Region (NLR), located above the plane of the torus along its symmetry axis.

The first AGNs were discovered in spiral galaxies, the so-called Seyfert galaxies (Seyfert 1943). Later, AGNs were also found in elliptical galaxies and in point-like Quasi-Stellar Objects (QSOs; or quasar). By now, AGNs have been found in nearly all galaxy types, including several ULIRGs.

1.4.1 Observable characteristics

Thanks to the presence of an extremely hot accretion disk in combination with a surrounding molecular torus, AGNs can be studied across the entire electromagnetic spectrum.

The central region produces copious X-rays which heat and ionize the surrounding gas and dust. Their X-ray continuum can be detected by X-ray satellites. Depending on the gas column density along the line of sight, the emission may, however, be weakened or blocked completely. The latter occurs for column densities N(H)$>10^{24.5}$ cm^{-2}, in which case the obscuring source is called 'Compton thick'. Type-2 Seyferts generally have higher columns than type-1 AGNs. More than 50% of nearby type-2 Seyferts even have columns N(H)$>10^{24}$ cm^{-2} (Risaliti et al. 1999).

At radio wavelengths, the presence of an AGN can be confirmed if the brightness temperature of the central source is higher than 10^6 K (Condon 1992). An AGN may, however, remain undetected if the source is radio-quiet or strongly synchotron self-absorbed.

In the mid-infrared, the presence of an AGN may be deduced spectroscopically in several ways. First, by the presence of high excitation fine structure lines like 3.93 μm [Si IX], 14.3 & 24.3 μm [Ne V] and 7.65 μm [Ne VI], resulting from ionization of gas by X-rays from the central source (e.g. Genzel et al. 1998; Sturm et al. 2002; Lutz et al. 2002). Second, by the presence of a mid-infrared continuum, resulting from heating the torus gas by the central X-ray source. AGN unification schemes predict the strength of this continuum to be weaker for type-2 than for type-1 AGNs, because of strong extinction by the intervening torus. Such a difference has indeed been observed by Clavel et al. (2000). It is important to emphasize that the central region of the AGN shows no evidence for PAH emission features (Sturm et al. 2000; Laurent et al. 2000), likely because these molecules have been destroyed in the X-ray irradiated environment.

Given the small diameter of the ISO telescope (60 cm), direct observation of the AGN continuum without strong contamination by emission from the host galaxy, has only been possible for the nearest AGNs. Fig. 1.9 shows the 5–16 μm spectra of the nearby AGNs Cen A and NGC 1068 (Laurent et al. 2000). As can be clearly seen, the spectra of the central regions are continuum-dominated, in sharp contrast to the spectra of the host galaxies, which are PDR-like. Note the difference in contrast of the AGN and PDR spectra between NGC 1068 and Cen A. The effect is entirely due to the far higher AGN continuum luminosity of NGC 1068.

1.5 ULIRGs at mid-infrared wavelengths

As illustrated by Fig. 1.2, ULIRGs emit the bulk of their luminosity in the infrared. Unfortunately, studying ULIRGs at these wavelengths is extremely difficult. Telescopes need to be cooled to near-zero temperatures, development of sensitive infrared detectors is technologically challenging and the atmosphere is opaque throughout most of the infrared spectral range. As a result, mid- and far-infrared astronomy lack the spatial and spectral resolution and the sensitivity of optical and near-infrared astronomy and require a space-based observatory. Until recently, most of our understanding of the processes at work in ULIRG nuclei was therefore based on studies at optical, near-infrared, millimeter and radio wavelengths. With the advent of the *Infrared Space Observatory* (ISO), mid-infrared spectroscopy became available as another tool to study the properties of ULIRGs. Below I summarize some of the results in the context of my thesis. For a more detailed overview, I recommend the review by

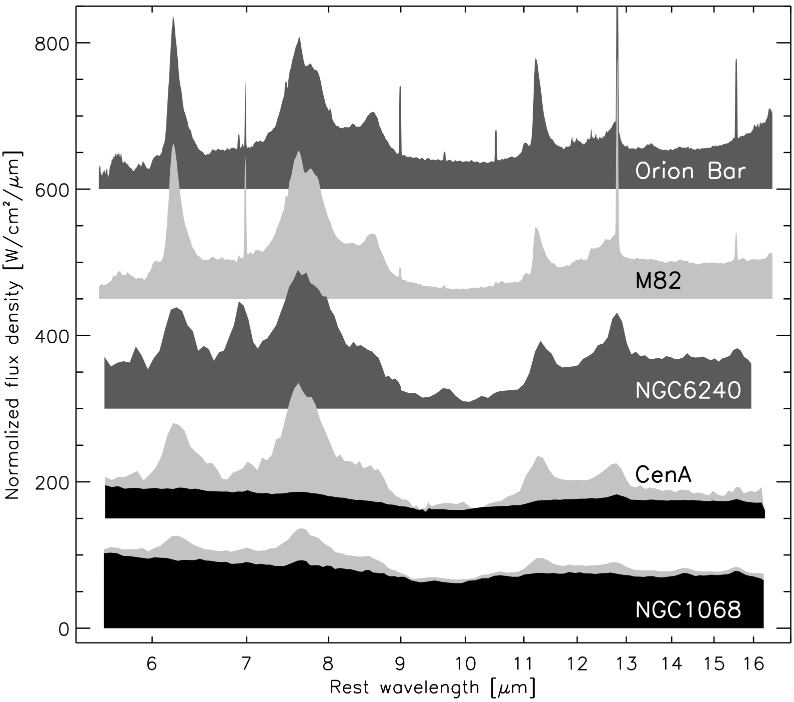

FIGURE 1.9 — 5–16 μm spectral energy distributions. The spectra have been scaled and offset. **Orion Bar:** The spectrum of the Orion Bar photo-dissociation region (Peeters et al. 2002a) is dominated by PAH emission features at 3.3, 6.2, 7.7, 8.6, 11.2 and 12.7 μm. **M 82:** The spectrum of the starburst core (Sturm et al. 2000) is like the spectrum of the Orion Bar dominated by PDRs. **NGC 6240:** The spectrum of the ULIRG NGC 6240 (Laurent et al. 2000) is dominated by PDR features. **Cen A:** The *black area* indicates the nuclear and the *grey area* the circumnuclear spectrum of Cen A (Laurent et al. 2000). **NGC 1068:** The *black area* indicates the nuclear and the *grey area* the circumnuclear spectrum of NGC 1068 (Laurent et al. 2000).

Genzel & Cesarsky (2000).

The near- and mid-infrared spectral range is extremely rich in ISM emission and absorption features. As the conditions of dust and gas depend strongly on the processing by nearby (forming) stars or the presence of an AGN, a detailed study of the spectral features will give insight in the nature of the sources responsible for the observed ISM conditions. This is maybe best illustrated by the two spectra in Fig. 1.4, which show the clearly different spectral appearance of embedded and exposed star formation.

ULIRG nuclei are known to be extremely dusty. Extinction estimates based on near- and mid-infrared hydrogen recombination lines and/or ratios of mid-infrared fine structure lines range from A(V)=5 to 50. The true extinction may, however, be far higher if emission and absorption components are mixed along the line of sight (Genzel et al. 1998). The nuclear power sources may remain hidden even at mid-infrared wavelengths. The nucleus of the nearby starburst/Seyfert-2 galaxy NGC 4945 (Fig. 1.1) offers an interesting testground in this respect, as hard X-ray observations have revealed the presence of a deeply enshrouded powerful AGN (e.g. Iwasawa et al. 1993), coexisting with an obscured nuclear starburst, which is responsible for a strong starburst superwind (Moorwood et al. 1996b).

As discussed in the previous Section, the spectral signatures of AGN activity are quite different from those of exposed star formation. Genzel et al. (1998) exploited these differences in an impressive mid-infrared study of 45 ULIRG, Seyfert and starburst nuclei and found that pure AGNs and starbursts separate well in a diagnostic diagram (Fig. 1.10) with on one axis the 7.7 μm-PAH feature-to-continuum ratio and on the other axis the ratio of a high to a low excitation line (e.g. [Ne V]/[Ne II] or [O IV]/[Ne II]). Most ULIRGs were found to be starburst-like in their 7.7 μm-PAH feature-to-continuum ratios and to have upper limits on their high-to-low excitation line ratios at the lower end of the AGN range. Genzel et al. (1998) concluded from this that ULIRGs are predominantly starburst powered. Fig. 1.9 shows the nuclear and galaxy-integrated mid-infrared spectra of two galaxies containing a type-2 AGN. In Cen A, circumnuclear star formation dominates the galaxy-integrated spectrum, while the AGN dominates the NGC 1068 spectrum. While this may be a true indication of the relative importance of AGN and starburst activity in these systems, the strength of the AGN continuum is known to vary by a factor $\sim$8, depending on the orientation of the AGN torus (Clavel et al. 2000). The importance of an AGN may hence be under- or overestimated by a factor $\sim$8 if the obscuration is not corrected for. Classification of galaxies in AGN- or starburst-dominated on the basis of just their 7.7 μm-PAH feature-to-continuum ratio should therefore be avoided.

Soifer et al. (2002) took a different approach to estimate the contribution of star formation to the total luminosity of ULIRGs. Assuming the ratio L(11.2 μm-PAH)/L(IR) for the nuclear starburst in M 82 to be typical for star formation elsewhere, they found that only 10% of the total luminosity of Arp 220 may be associated with exposed star formation. This fraction is far smaller than the >50% estimated from the 7.7 μm PAH line-to-continuum ratio (Genzel et al. 1998; Lutz et al. 1998; Rigopoulou et al. 1999; Tran et al. 2001).

1.6 In this thesis

A key question in astronomy is the interrelationship of mergers, starburst and AGN activity. In this thesis, I have focussed on infrared observational diagnostics of the energetic phenomena in the nuclei of (U)LIRGs and the insight they provide in the ultimate energy source of such objects.

In Chapter 2, I present the sample of mid-infrared galaxy spectra used in this thesis. The sample comprises $\sim$ 250 spectra of normal galaxies, starburst galaxies, Seyferts, QSOs, ULIRGs and HyLIRGs. These spectra were obtained with all three mid-infrared spectrometers onboard ISO: SWS ($R\sim$1500), PHT–S ($R\sim$90) and CAM–CVF ($R\sim$35). I examine the spectra for the presence of ice absorption features. This results in the detection of ice in 18 galaxies and in an ice galaxy classification, which may also represent an evolutionary sequence.

Chapters 3 and 4 present a near- and mid-infrared case study of the nearby starburst/Seyfert-2 galaxy NGC 4945. The observations reveal strong absorptions by ices and silicates towards the nuclear starburst. Solid CO_2, CO and OCN^- are detected for the first time in an external galaxy. The profile of the solid CO band reveals the importance of thermal processing of the ice, while the prominence of the OCN^- band attests to the energetic processing of ices by FUV radiation and/or energetic particles. We find no spectral evidence for the existence of a powerful AGN, inferred from hard X-ray observations.

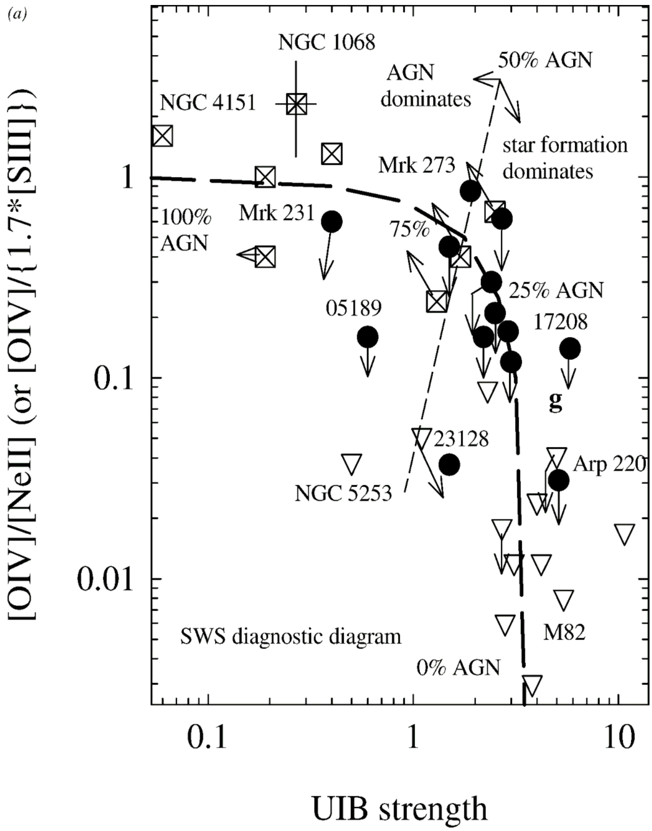

FIGURE 1.10 — Genzel diagram (Genzel et al. 1998). The vertical axis measures the flux ratio of high excitation to low excitation mid-infrared emission lines, and the horizontal axis measures the strength (i.e. feature to continuum ratio) of the 7.7 μm-PAH feature. AGN templates are marked as *rectangles with crosses*, starburst templates as *open triangles*, and ULIRGs as *filled circles*. A simple mixing curve from 0% to 100% AGN is shown with *long dashes*.

In Chapter 5, the exotic mid-infrared spectrum of NGC 4418 is presented. In contrast to the spectra of most other LIRGs, the spectrum of NGC 4418 reveals no sign of PAH emission features, but is dominated instead by deep absorption features of ices and silicates. From the depth of the ice features we infer that the powerful central source responsible for the mid-infrared spectrum must be deeply enshrouded.

In Chapter 6, the 6–12 μm spectrum of Arp 220 is re-analyzed. The spectrum is not consistent with a scaled-up version of a typical starburst, but may instead be the superposition of an NGC 4418-like absorbed continuum source and a weakly absorbed starburst spectrum. Consequences for the starburst energy budget are discussed.

In Chapter 7, I investigate the role of PAHs as a tracer of star formation, based on a sample of Galactic regions of massive star formation. For this purpose, I define a MIR/FIR diagnostic diagram of far-infrared normalized 6.2 μm PAH flux versus far-infrared normalized 6.2 μm continuum flux. Within this diagram the Galactic H II regions span a sequence from embedded compact H II regions to exposed PDRs. The extragalactic sample is compared to these Galactic sources. I also investigate if PAHs are good tracers of star formation.

Finally, the results from the research presented in this thesis and its main conclusions are summarized in Chapter 8.